crystals

MDPI

Review

Protein Dynamics and Time Resolved Protein Crystallography at Synchrotron Radiation Sources: Past, Present and Future

Jose M. Martin-Garcia

Department of Crystallography and Structural Biology, Institute of Physical Chemistry Rocasolano, Spanish National Research Council (CSIC), 28006 Madrid, Spain; jmmartin@iqfr.csic.es

Abstract: The ultrabright and ultrashort pulses produced at X-ray free electron lasers (XFELs) has enabled studies of crystallized molecular machines at work under 'native' conditions at room temperature by the so-called time-resolved serial femtosecond crystallography (TR-SFX) technique. Since early TR-SFX experiments were conducted at XFELs, it has been largely reported in the literature that time-resolved X-ray experiments at synchrotrons are no longer feasible or are impractical due to the severe technical limitations of these radiation sources. The transfer of the serial crystallography approach to newest synchrotrons upgraded for higher flux density and with beamlines using sophisticated focusing optics, submicron beam diameters and fast low-noise photon-counting detectors offers a way to overcome these difficulties opening new and exciting possibilities. In fact, there is an increasing amount of publications reporting new findings in structural dynamics of protein macromolecules by using time resolved crystallography from microcrystals at synchrotron sources. This review gathers information to provide an overview of the recent work and the advances made in this filed in the past years, as well as outlines future perspectives at the next generation of synchrotron sources and the upcoming compact pulsed X-ray sources.

Keywords: protein dynamics; time-resolved serial crystallography; synchrotrons; XFELs; microcrystals

Citation: Martin-Garcia, J.M. Protein Dynamics and Time Resolved Protein Crystallography at Synchrotron Radiation Sources: Past, Present and Future. *Crystals* **2021**, *11*, 521. https://doi.org/10.3390/cryst11050521

Academic Editors: Oliviero Carugo and Ki-Hyun Nam

Received: 28 March 2021
Accepted: 4 May 2021
Published: 8 May 2021

1. Introduction

"Watching" biological macromolecules in action at atomic resolution rather than just being limited to 3D-dimensional static pictures, has been the *holy grail* for structural biologists since the first high-resolution structure of an enzyme was solved [1]. The technique of time-resolved crystallography is an experimental technique that detects molecular changes at atomic and temporal resolutions [2], providing the opportunity to bring the dimension of time into the crystallographic experiment. Historically, time-resolved macromolecular crystallography at ambient temperature has been conducted on large single crystals using Laue diffraction techniques (see review [3]). The pink X-ray beam (or polychromatic beam) used in the Laue technique offers an average photon flux 100 times higher than the monochromatic beams and is coupled with the 100 ps time-resolution capability, which provides a dependable platform for probing structural intermediates of essential biological macromolecules. Pioneered by Moffat and colleagues [4–11], the Laue method has been applied to the study of photoreceptor intermediates, ligand photolysis and allosteric action in heme proteins, enzymatic reactions, ligand–enzyme interactions, viruses, and viral drug complexes [12–16]. Due to the feasibility of rapid reaction initiation by a laser pulse, this technique has been widely used to study light-active protein systems including myoglobin [17], hemoglobin [7], photoactive yellow protein [18–20], photosystem II [21–26] and bacteriorhodopsin [27–29].

The higher X-ray flux of the pink X-ray beam along with the broad bandwidth, which leads to a high fraction of fully integrated Bragg peaks recorded in a snapshot pattern and a greater coverage of reciprocal space, are advantages that have long been appreciated for

time-resolved Laue diffraction experiments at synchrotron facilities [30]. The increased bandwidth used in the Laue crystallography has two benefits over the monochromatic X-ray beams used in conventional crystallography: (1) reflections falling within the limiting Ewald spheres are fully recorded, so that one can avoid rotating the crystals during X-ray data collection; and (2) more reflections fall within the Ewald sphere so that only a few diffraction patterns are needed to collect a complete data set. On the other hand, Laue crystallography has also a big disadvantage, its high sensitivity to crystal mosaicity. The broad bandwidth of the pink X-ray beam makes reflections become streaky and sparse, so that data processing fails using Precognition (Renz Research Inc; https://biocars.uchicago.edu/facilities/software/precognition-documentation/), the most widely used Laue data processing software. The signal-to-noise ratio (SNR) of a given reflection decreases if the increasing bandwidth leads to increased intensity because the background scattering is proportional to the incident intensity. So, the ideal bandwidth to fully record reflections with maximum SNR is probably slightly larger than that required to match the crystal mosaicity. Despite this disadvantage, the technique of Laue crystallography has rapidly evolved over the past 25 years with developments in cryo-technology, tunable lasers, increased computing power and vastly improved X-ray detectors, as well as synchrotron radiation itself, which has allowed the technique to move from the millisecond [5] to the picosecond temporal resolution regimes [18]. While this technique continues to improve, it faces some hard limitations due to the nature of large crystals and current synchrotron sources, namely: (1) temporal resolution is limited by pulse length achievable using a synchrotron; (2) irreversible reactions cannot be studied as the induction of a reaction would cause a permanent modification of the molecules in the crystal; (3) only light activated, pump-probe type experiments are generally feasible at present, with limited light penetration being one of the major obstacles; and (4) homogeneity of reaction initiation must be considered and presents a challenge.

The field of structural biology is continuously evolving and experiencing numerous technological breakthroughs that are rapidly accelerating not only the 3D structure determination of macromolecules but also structural dynamics. Among these advances are the high-brightness and high repetition rate of photon sources such as X-ray free electron lasers (XFELs). In 2009, XFELs came into play producing extraordinarily powerful and ultrashort X-rays to take diffraction snapshots of nano- or micro-crystals at room temperature on the fly before they are destroyed by the so called, serial femtosecond crystallography (SFX) technique, with the potential to make molecular movies and discover how macromolecules work. The major challenge in the field of time-resolved X-ray crystallography has been the study of irreversible reactions, which can be initiated by a flash of light or by diffusion of a substrate into the crystal lattice of a macromolecule. Recent advances in sample delivery technology and XFELs have allowed time-resolved serial femtosecond crystallography (TR-SFX) to be extended to other systems as well [31–33]. Stagno and co-workers reported TR-SFX data that demonstrate the binding of adenine to a riboswitch, an aptamer of messenger RNA that regulates gene expression. In this study, the crystallographic structures of the adenine riboswitch aptamer domain during the course of the reaction mechanism (two unbound apo structures, one ligand-bound intermediate and the final ligand-bound conformation) were determined using mix-and-inject technologies at an XFEL [33]. It has also recently been demonstrated that the binding of an antibiotic to an enzyme can be studied by collecting data at room temperature using time-resolved SFX at LCLS [31,32]. Such studies have remained largely elusive at synchrotron sources because of X-ray radiation damage, the need for growing large single crystals, challenges with crystal replenishment, and the difficulty in initiating reactions uniformly in macroscopic crystals.

The transfer of the serial crystallography approach to next-generation synchrotrons upgraded for higher flux density and with beamlines using sophisticated focusing optics, submicron beam diameters and fast low-noise photon-counting detectors offers a way out of this conundrum. In applications such as room-temperature data collection or phasing from radiation-sensitive microcrystals, SMX at synchrotrons has developed into a viable

alternative in the past seven years with 41 SSX experiments carried out, so far, at these facilities (see Table 1). At present, almost each one of the most powerful synchrotrons has at least one microfocus beamline (see Table 1) that offers the SSX capability and can be developed into a routine method for room-temperature structure determination of macromolecules. This successful adaptation of SX at synchrotrons has been mostly feasible due to the rapid advances in sample delivery technology (see review by [34], which reduces sample consumption significantly compared to liquid jets.

Even though serial crystallography (SX) techniques were originally developed for the XFEL, there is growing interest in pursuing SX at synchrotron sources where beam time availability is not as scarce. Early SSX experiments implied the use of viscous jets [35,36]. However, recent advances in sample delivery methods have extended its use to more types of proteins, protein complexes, as well as opened-up the possibility of conducting time-resolved SX experiments at synchrotrons. Serial methods can provide vital insight into challenging areas such as room temperature studies, protein dynamics and overcoming problems from radiation damage. This review focuses on the latest results of enzymatic reactions that are activated by light. It also highlights the most recent advances towards developing the first mix-and-inject time-resolved experiments at synchrotrons.

2. Some Important Considerations for Time-Resolved Crystallography Experiments

The serial femtosecond crystallography (SFX) technique has increased the number of structures of macromolecules in the PDB with 383 currently deposited as of 1 May 2021, as well as expanded the information that can be obtained from them regarding structural dynamics (see review [37]). The high solvent content and the weak forces that stabilize crystal contacts typically present in macromolecular crystals, have always been a challenge to obtain large and well-diffracting crystals. However, the porous nature of macromolecular crystals with large solvent channels has allowed for slight conformational movements of the proteins, and the diffusion of ligands (substrates and antibiotics) to the active site within crystals, being an opportunity to "watch" structure of intermediate states along an enzymatic reaction [31–33]. Thus, it is now possible to understand the relationship between structure and function of macromolecules by time-resolved SFX (TR-SFX) studies, in which numerous structures along a reaction pathway can be determined. This approach has potential applications in the field of structure-based rational design, renewable energy and photosynthesis by unraveling the mechanism of biological processes.

However, some important considerations must be considered before carrying out reliable time-resolved experiments: (1) The way in which data is collected must be considered, especially when studying irreversible reactions [38]. For instance, in traditional X-ray crystallography, data sets are collected as crystals are rotated so that each diffraction pattern collected corresponds to a rotational increment of the reciprocal space. Thus, for an irreversible reaction in which crystals are permanently altered after the induction of the reaction, one would require lots of relatively large crystals and multiple crystal settings for each time point, in order to collect a complete data set. However, the serial nature of SFX experiments, with one diffraction pattern collected from each individual microcrystal, bypasses this limitation by the development of new data processing methods to recover the integrated X-ray intensities from the partial reflections recorded in SFX. The integrated intensities are merged from thousands of snapshots for each indiviudal reflection collected from individual microcrystals in random orientations, leading to accurate structure factors for time-resolved experiments. This approach is called Monte Carlo integration [39,40]. In SFX, an iterative process of hit finding and indexing is typically done until a sufficiently large number of indexable diffraction patterns is identified [41–43].

Table 1. SMX experiments carried out at synchrotron radiation sources. TR-SSX experiments are highlighted with asterisk.

Exp. #	Machine	Beamline	Delivery Method	Protein/Substrate	Temp.	Resol. (Å)	PDB Code	Ref.
1	PETRA III	P14	Cryo-loop	Cathepsin B	100 K	3.00	4N4Z	[44]
2	PETRA III	P11	Glass-capillary	Lysozyme	293 K	2.10	4O34	[45]
3	CHESS	F1	Microfluidic/chip	Glucose Isomerase (GI)	293 K	2.1	Not deposited in PDB	[46]
4	ESRF	ID13	Silicon nitride chip	Lysozyme	293 K	1.95	4WL7	[47]
5	SLS	X10SA	High-viscosity injector	Lysozyme	293 K	1.90	4RLM	[35]
6	ESRF	ID13	High-viscosity injector	Bacteriorhodopsin (bR)	293 K	2.40	4X31	[36]
7	APS	23-ID-D	Silicon nitride chip	Lysozyme	293 K	1.55	4Z98	[48]
8	SLS	X10SA	Cyclic olefin copolymer (COC) sandwich plates	Lysozyme	100 K	1.8	4XJD	[49]
				Alginate Transporter (AlgE)	293 K	2.8	4XNI	
				Petptide Transporter (PepT)	293 K	2.9	4XNK	
9	ESRF	ID29	Cryo-loop	Lysozyme	100 K	1.6	5A3Z	[50]
				Thermolysin		1.3	5A3Y	
				Bacteriorhodopsin (bR)		2.5	5A44	
				Thaumatin		1.2	5A47	
10	DLS	I24	Silicon chip	Thaumatin	293 K	2.2	Not deposited in PDB	[51]
				Proteinase K		2.1		
11	DLS	I24	Silicon chip	Polyhedrin	293 K	1.5	4X35	[52]
				Lysozyme		2.1	4X3B	
12	SLS	X06SA/X10SA	Cyclic olefin copolymer (COC) sandwich plates	Lysozyme	100 K	1.7	5D5C	[53]
				Insuline		1.5	5D53	
				Alginate Transporter (AlgE)		2.4	5D5D	
				Petptide Transporter (PepTst)		2.4	5D58	
				Diacylglycerol kinase (DgkA)		2.8	5D56	
				β_2-adrenergic receptor (β_2AR)		2.5	5D5A	

Table 1. *Cont.*

Exp. #	Machine	Beamline	Delivery Method	Protein/Substrate	Temp.	Resol. (Å)	PDB Code	Ref.
13	DLS	I03	Silicon chip	Insulin	293 K	1.9	5FB6	[54]
14	Spring-8	BL41XU	Loop	Luciferin	107 K	1.6	5GX1	[55]
15	APS	23-ID-D	High-viscosity injector	Adenosine A_{2a} Receptor (A_{2a}AR)	293 K	3.1	5UVI	[56]
				Phycocyanin		3.2	5UVK	
				Lysozyme		2.1	5UVJ	
				Proteinase K		2.6	5UVL	
16	APS	14-ID-B	Chip	Phycocyanin	293 K	2.1	5MJP	[57]
				Proteinase K		2.2	5MJL	
17	PETRA III	P11	Tape-drive	Lysozyme / Chitotriose (CTO)	293 K	1.7	5JNP, 5NJQ, 5JNR, 5JNS	* [58]
18	SLS	X06SA	High-viscosity injector	Adenosine A_{2a} Receptor (A_{2a}AR)	293 K	2.1	5NLX	[59]
				Lysozyme		1.5	5NMJ	
				αβ-tubulin-darpin Complex (TD1) / Colchicine		2.1	5NQT	
				Molybdenum Storage Protein (MOSTO)		7.7	5OW5	
19	SLS	X10SA	High-viscosity injector	Thermolysin	293 K	2.3	Not deposited in PDB	[60]
				Glucose Isomerase (GI)		2.0		
				Lysozyme		1.9		
				Bacteriorhodopsin (bR)		2.3		
20	ANSTO	MX2	Micro-mesh	Bombyx mori cytoplasmic polyhedrosis virus 1 (BmCPV1)	300 K	1.51.9	5EXY, 5EXZ	[61]
21	ESRF	ID23-2	Micro-mesh chips	Thaumatin	100 K	2.1	5FGT	[62]
				Insulin		1.7	9INS	
22	PETRA III	P11	High-viscosity injector	Proteinase K	293 K	1.9	6FJS	[63]

Table 1. *Cont.*

Exp. #	Machine	Beamline	Delivery Method	Protein/Substrate	Temp.	Resol. (Å)	PDB Code	Ref.
23	NSLS-II	FMX	Regular loops meshes	Proteinase K	100 K	2.0	Not deposited in PDB	[64]
				Trypsin		1.5		
24	NSLS-II	FMX	Micro-well-mounts	Thaumatin	100 K	2.5	6C5Y	[65]
25	PETRA III	P14	Microfluidic chips	Thaumatin	293 K	1.9	1LR2	[66]
				Glucose Isomerase (GI)		1.7	4ZB2	
				Thioredoxin		3.0	4FYU	
26	APS	14-ID-B	Quartz chips	Ultraviolet-B receptor (UVR8)	293 K	2.0	6DD7	[67]
				Photolyase PhrB		2.3	6DD6	
27	PETRA III	P14	Hit And Return (HARE) chip	Fluoroacetate dehalogenase (FAcD) / Photocaged fluoroacetate	293 K	1.8	6GXH, 6FSX, 6GXD, 6GXT, 6GXF, 6GXL	* [68]
28	SLS	X06SA	Cyclic olefin copolymer (COC) sandwich plates	Petptide Transporter (PepTst)	100 K	2.6	Not deposited in PDB	[69]
29	APS	14-ID-B	High-viscosity injector	Adenosine A_{2a} Receptor (A_{2a}AR)	293 K	4.2	6MH8	[70]
				Proteinase K		1.8	6MH6	
30	SLS	X06SA	High-viscosity injector	Bacteriorhodopsin (bR)	293 K	1.8–2.3	6RQP, 6RQO, 6RNJ,6RNH	* [29]
31	PETRA III	P14	Liquid Application Method for time-resolved Analysis (LAMA) chip	Lysozyme / Chitotriose (CTO)	293 K	1.7–1.8	6RNB, 6RNC, 6QNB	* [71]
				Xylose Isomerase (XI) / Glucose		1.7–2.0	6QNH, 6RND, 6RNF, 6QNC, 6QNI, 6QNJ, 6QND	
32	PETRA III	P11/P14	Hit And Return (HARE) chip	Fluoroacetate dehalogenase (FAcD) / Photocaged fluoroacetate	293 K	1.7–1.9	6QHY, 8QHV, 6QHU, 6QHT, 6QHS, 6QHQ, 6QHP, 6QHW, 6QHZ, 6QI0, 6QI1, 6Q12, 6QI3	* [72]
33	ESRF	ID13	Microfluidic device	Lysozyme	293 K	2.1	6H79	[73]
34	ESRF	ID30A-3	Goniometer/loops	Phototropin-2	293 K	2.2–2.9	6S45, 6S46	*# [74]

Table 1. *Cont.*

Exp. #	Machine	Beamline	Delivery Method	Protein/Substrate	Temp.	Resol. (Å)	PDB Code	Ref.
35	ESRF	ID30A-3	Microfluidic device	Aspartate α-decarboxylase (ADC)	293 K	2.0	6RXH	[75]
				Lysozyme		2.0	6RXI	
36	SSRF	18U1	Microfluidic plate	Lysozyme	293 K	2.2	7C09	[76]
				Proteinase K		2.1	7C0P	
37	ESRF	ID13	Silicon chip	Lysozyme	293 K		6Q8T, 6Q88	[77]
38	ALBA	XALOC	High-viscosity injector	Rhodopsin KR2	293 K	2.5	6YC0	* [78]
39	PETRA III	P14	Loops	Glycine transporter 1 (GlyT1)	100 K	3.4–3.9	6ZBV, 6ZPL	[79]
40	Spring-8	BL41XU	Polyimide mesh loop	Lysozyme	293 K	1.7–1.8	7CDK, 7CDM, 7CDN, 7CDP, 7CDQ, 7CDR, 7CDS, 7CDT, 7CDU	[80]
41	PETRA III	P14	Hit And Return (HARE) chip	Fluoroacetate dehalogenase (FAcD)	293 K	1.7	7A42	[81]
				Myoblobin			7A44	

[#] Despite data sets from t = 0 ms to t = 4.1 s were collected, only two crystal structures corresponding to initial (t = 0 ms) and final (t = 4.1 s) states and were deposited in the PDB.

(2) Structural homogeneity and the constraint of Laue crystallography to mostly pump-probe type experiments are closely connected due to one parameter, diffusion [38]. Until recently, Laue crystallography has always been limited to photo-activated reactions since chemically activated ones would necessitate the diffusion of a ligand (substrate or antibiotic) throughout large crystals, which limits the reaction time scales currently available. Assuming the active site of a macromolecule is unobstructed and the substrate is sufficiently small, the large solvent channels present in macromolecular crystals may allow for diffusion of ligands via soaking approaches [82–84]. However, the relatively large size of the crystals used in Laue crystallography would limit diffusion times, constraining the accessible time resolution regime of reaction intermediates in an experiment. Despite this limitation, there have been chemically activated time-resolved experiments performed successfully by incorporating photo-activated caged ligands into large crystals by either soaking or co-crystallization techniques [85–87]. However, in contrast to Laue crystallography, the tiny size of the crystals used in SFX allow for diffusion times on the order of millisecond time scales, allowing access to many reactions on the short millisecond regimes without the need of using photo-caged ligands [88]. (3) Reaction homogeneity throughout the crystals [39]. Despite reaction initiation is more homogeneous and rapid in photo-activated reactions than in diffusion-based reactions, the degree of reaction initiation by photoinduction is also limited by the size of the crystals since protein macromolecules absorb light as it travels through the crystal, which results in a decrease in transmission of light as the crystal size increases. As pointed out by Martin-Garcia et al., the reaction homogeneity of the molecules inside large crystals is sensitive to the lifetime of an intermediate state as compared to the time difference of reaction initiation between the front and back surfaces of the crystal relative to the pump laser [38]. The distance traveled by light between the front and back of photo-activated crystals is not the main cause of this temporal offset but the attenuation of its intensity as it proceeds through the crystal due to absorption and scattering processes [38]. This could be addressed by just increasing the power of the laser; however, this practice could lead to severe photo-damage and heating effects inside the crystals. However, the tiny size of the crystals used in TR-SFX provides a big advantage over large crystals since they allow for a much smaller difference of reaction initiation throughout the tiny crystals and, thus, requiring less pump laser intensities for maximal reaction initiation. In addition, the volume of the microcrystals is so small that nearly the entire crystal is illuminated by the laser, which minimizes the intensity profile of the pump laser. These considerations make TR-SFX to provide with the basis for a much higher reaction initiation yield, a point that has already been shown in practice [19].

3. Time-Resolved Serial Femtosecond Crystallography (TR-SFX)

Time-resolved crystallography (TRX) has historically been performed on large single crystals by Laue pink X-ray beam diffraction (for a review see [3]) and has exhibited considerable gains over the past 25 years, moving from the millisecond [5] to the picosecond [18] temporal resolution regimes, opening the door to observing conformationally dynamic proteins in action at atomic scale. However, while this technique continues to improve, it has two main limitations: (1) the time resolution currently achievable with even the best synchrotron radiation source is limited by the X-ray pulse length of approximately 100 ps; and (2) it requires a rapid reaction initiation that quickly spreads uniformly across all molecules in the crystals and with high efficiency, and this represents a clear challenge with large crystals. Due to these two limitations, irreversible reactions are impractical by Laue crystallography as the induction of a reaction would cause a permanent modification of the protein molecules in the crystal, thus, only pump-probe experiments with light-activated proteins or enzymatic reactions with photo-caged substrates are currently feasible.

Thus, the serial "diffraction before destruction" nature of SFX experiments along with the short pulse durations of X-ray beams produced at XFELs, complements the Laue method by accessing to experiments previously impossible bypassing the above challenges. The short pulse durations of X-ray beams produced at XFELs, on the order of tens of fem-

toseconds, allows us to detect and resolve time points in fast catalytic reaction processes so that, more temporally constrained intermediates can be detected along a reaction pathway. In addition, SFX use small crystals allowing for much faster diffusion times on microsecond time scales compare to second time scales of large crystals [89], thus, time-resolved SFX (TR-SFX) permits access to reactions that occur on the short millisecond and even microsecond regimes, providing time-lapse snapshots of transient intermediates. Initial, intermediate and final state(s) can then be viewed in a quick succession from start to finish to reveal motion of the enzyme "in real time" to unravel how macromolecules proceed in nature. To date, numerous TR-SFX experiments have been carried out successfully on both light-activated and rapid-mixing reactions. Examples of the most relevant and exciting discoveries in the emergent technology of TR-SFX at XFELs have been gathered in a recently published review [37].

4. Time-Resolved Serial Synchrotron Crystallography (TR-SSX)

The limited availability of XFEL beamtime along with the highly demand and complexity of the SFX experiments, the continuous developments in hardware at synchrotrons with faster detectors and brighter microfocus beams, have targeted standard synchrotrons beamlines to become an alternative to perform serial crystallography experiments at these light sources. The successful adaptation of this approach at synchrotrons has been possible mostly due to the development of low sample consumption sample delivery methods such as the use of high-viscosity media, fixed targets, and hybrid devices. Liquid jets are not suitable for SSX due to the very short residency time of crystals in the X-ray interaction region as a result of the fast flow rates. As of April 2021, 41 SSX experiments have been conducted at synchrotrons using exposure times of a few milliseconds (Table 1). Almost every one of the 3rd and 4th generation synchrotrons have at least one macromolecular beamline that may offers the serial data collection approach as a routine method for room-temperature structure determination of proteins and its complexes. As shown in Table 1, most of the SSX experiments reported the structure determination of static protein structures, however, there exist a lot of interest in re-engineering the current sample delivery methods to be able to carry out time-resolved SSX (TR-SSX) at synchrotrons. For TR-SSX, one must consider the speed of the reaction initiation as well as the speed at which the sample is probed. The former requires sample delivery methods that can efficiently deliver tens of thousands of crystals into the X-ray beam and allow for rapid reaction initiation, either by a laser light pulse or by rapid mixing, before the sample is probed by the X-rays. The latter is a direct function of the beamline chosen for the experiment, being what has so far limited the achievable time-resolution to the millisecond domain for monochromatic microfocus beamlines at synchrotrons. However, higher time-resolutions can be achievable using pink X-beam SSX, offering the possibility to record data with time-resolution as short as 100 ps [57,70]. So far, just a few examples of TR-SSX experiments have been reported (Table 1), which will be highlighted in sections below.

5. Examples of Time-Resolved Experiments at Synchrotrons

5.1. TR-SSX with Viscous Jets

Originally developed to deliver crystals of membrane proteins embedded in lipidic cubic phase (LCP) at XFELs [90], the use of the high-viscosity injectors was quickly extended to deliver crystalline samples of more type of proteins including membrane and soluble proteins as well as protein complexes at synchrotrons. Taken advantage of the extremely low sample consumption of the injector-based approach, SSX with viscous jets has become, along with fixed target approach, the most used sample delivery method at synchrotrons (Table 1). The SSX with high-viscosity injectors has demonstrated to have important applications such as: (1) structure determination of membrane proteins [29,36,56,78]; (2) structure determination of novel protein complexes of pharmacological targets [59,60]; and (3) de novo phasing approaches [63]. However, and thanks to the possibility of collecting data at room temperature, which is key in the elucidation of protein dynamics, another im-

portant application of the viscous jet-based approach is the time-resolved pump-probe crystallographic studies, TR-SSX.

An example of this was reported recently by Standfuss and co-workers for bacteriorhodopsin protein [29]. The pump-probe SMX experiment resulted in a series of snapshots at time points from 0 ms to 15 ms upon light activation. This experiment was conducted on beamline X06SA at SLS synchrotron. Large structural rearrangements were observed in one of the helices, opening the cytoplasmic side and leaving a big gap that leads to the formation of a network of water molecules connecting the intracellular Asp96 with the retinal Schiff base (Lys216). The formation of this proton wire recharges the protein pump with a proton for the next cycle [29]. The results of this work, along with those previously obtained at XFELs for the mechanisms of the isomerization of the retinal chromophore, as well as that of the proton-released [27,28], clearly manifests the perfect synergy between synchrotrons and XFELs, and provides a complete picture of the mechanism of a biological pump. Figure 1 illustrates the results obtained from this experiment.

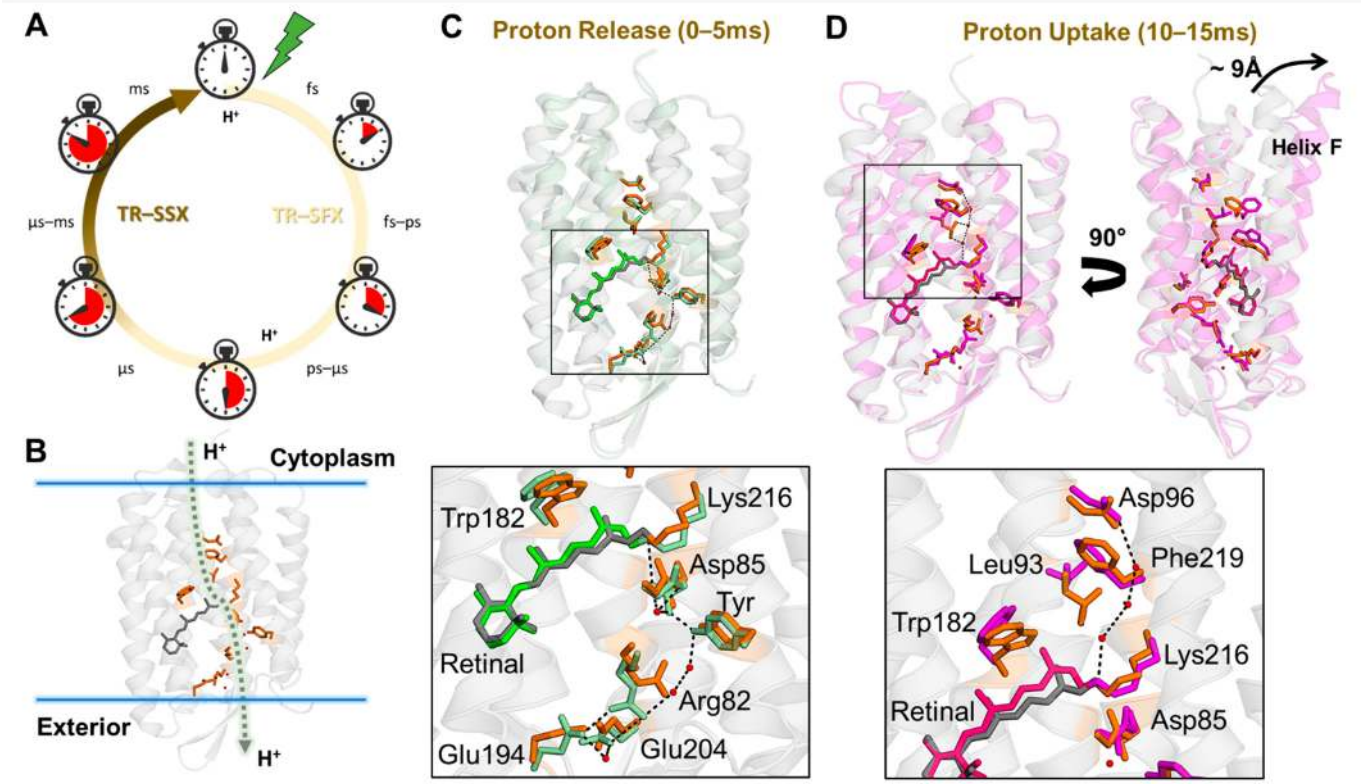

Figure 1. TR-SSX experiments for bR with viscous jets. (**A**) Proton pumping photocycle in bR with the relevant time domains for the individual steps. (**B**) Overview of the three principal steps in the photo cycle of bR. Structure of bR highlighting the key residues that participate in proton exchange from the cytoplasm to the exterior of the cell. Dashed arrow indicates the proton-transfer steps between charged residues. (**C**) Proton released step captured at 0–5 ms timepoint shows the rearrangements occurring at the necessary for proton release. The dark state is shown in orange and the closed state (0 to 5 ms) is shown in green. The red arrows indicate the direction of proton transfer reaction. (**D**) Proton uptake step captured at 10 to 15 ms timepoints in which the opening of the hydrophobic barrier between the primary proton donor Asp96 to the Shiff Base. The dark state is shown in orange and the open state (10 to 15 ms) is shown in pink. The conformational changes are accompanied by network of three water molecules (red spheres). The red arrows indicate the direction of proton transfer reaction. The displacement of about 9Å occurring on the cytoplasmic side at the end of helix F is also shown.

An unresolved matter of the viscous jets is the possibility of conducting mix-and-inject time-resolved experiments. The viscous jet-based approach has two drawbacks, the high-viscosity of the media and the jet speed currently achievable with this type of injectors, making the mix-and-inject approach for time-resolved experiments more

complicated. The naturally viscous consistency of the viscous media impedes ligands to quickly diffuse into de crystals making time-resolved experiments impractical. Despite the above limitations, SSX with viscous jets has been shown to be suitable for ligand soaking as demonstrated when mixing the substrate colchicine with TD1 microcrystals [59] and heavy metals into Lysozyme crystals as a proof-of-concept for the "de novo" single anomalous data (SAD) phasing [35] in LCP medium. However, there exists a lot of interests in making high-viscosity injectors suitable for time-resolved studies. Indeed, there are a few groups currently working on advancing injector technology in order to make the high-viscosity injectors suitable for mix-and-inject time-resolved studies.

5.2. TR-SSX with Fixed Targets

In this sample delivery approach, crystals are immobilized on a solid support and then scanned through the X-ray beam. They offer a variety of advantages, namely: (1) high hit rates; (2) low sample consumption; and (3) they can be used at room temperature and cryogenic temperatures. However, they also have some drawbacks such as a relatively high background caused by the solid support itself and the excess of mother liquor, high preferential orientation of the sample on matrix, and low repetition rates limited by mechanical aspects. Fixed target devices have rapidly evolved in the past 2–3 years with the development of two sample holders, the hit-and-return (HARE) system and the liquid application method for time-resolved analysis (LAMA), which allow for efficient data collection of time-resolved experiments at 3rd and 4th generation synchrotrons sources.

5.2.1. The HARE System

Schulz and co-workers recently introduced a newly designed fixed-target-based method using Si chips mounted on a high-speed translation stage that allows for time resolutions on the range from milliseconds to seconds and longer in pump-probe TR experiments [68]. The HARE is a very versatile system that allows for a large variety of time delays, covering large time windows that can go from 30 ms to 30 s. This is, in turn, a limitation of the HARE system since it is restricted to sampling time points that are mechanically encoded in the chip pattern and the acceleration of the translational stages. Despite this limitation, the HARE system can be used to study a large variety of reaction mechanisms as it covers the complete turnover cycle of most light-triggered enzymes. The proof-of-concept pump-probe time-resolved experiments were conducted at beamline P14 at PETRA III using fluoroacetate dehalogenase (FAcD) from *Rhodopseudomonas palustris* as sample [68,72]. Microcrystals of FAcD were mixed with an inactive version of the natural substrate of FAcD, a photocaged fluoroacetate, which can undergo a fast photocleavage upon illumination with UV light produced by a femtosecond laser. In the first experiment by Schulz et al. 2018, intermediates of the reaction of FAcD with fluoroacetate were successfully captured at three-time delays, 30 ms, 752 ms and 2 s, demonstrating the suitability of this approach [68]. In the follow up experiment by Merhabi et al. 2019, the HARE method was applied to further understand the allostery and dynamics of FAcD with fluoroacetate over the course of the full catalytic reaction as a function of time [72]. A total of 18 high-resolution crystal structures were determined at time delays between 30 ms and 30 s. From this experiment, the binding of the substrate to the active site of FAcD, all conformational changes occurring during the accommodation of the substrate within the active site, the positioning of a water molecule for hydrolysis of the intermediate, as well as the formation, release of the final product and regeneration of the enzyme, were seen for the first time ever. Figure 2 illustrates the whole reaction pathway.

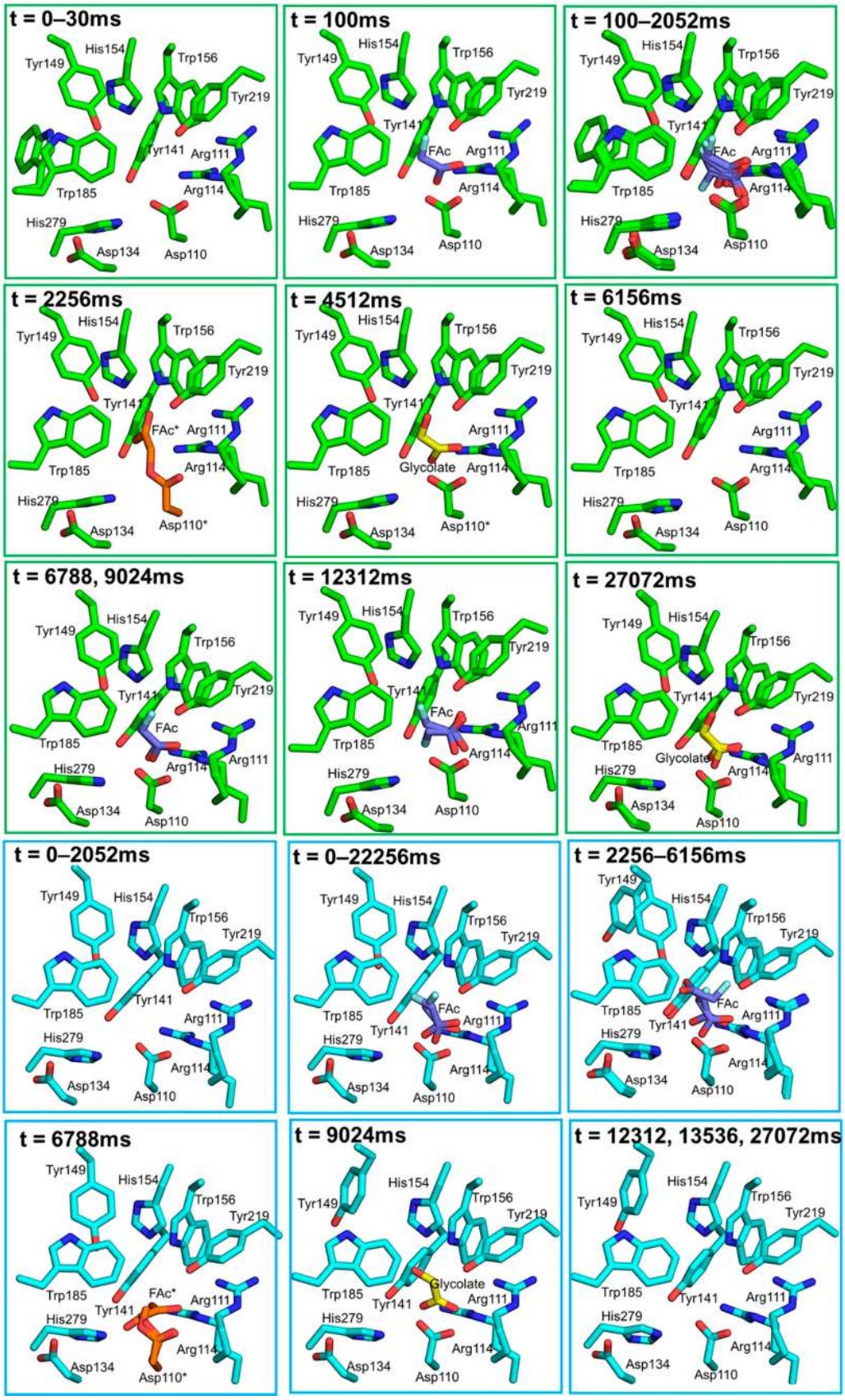

Figure 2. TR-SSX for FAcD with HARE system. All changes occurring at both catalytic sites of FAcD (green boxed for protomer (**A**) and blue boxed for protomer (**B**) captured during the experiment are represented. The key residues at the catalytic site, the substrate (FAc) and the product (glycolate) are highlighted and represented as sticks.

5.2.2. The LAMA System

Typically, in rapid mixing approaches, a substrate and a crystals slurry are mixed and delivered to the X-ray beam either as liquid jets [31–33,90] or on a tape-drive device (see Section 5.3). However, the major limitation of all these liquid-mixing techniques is the reduced minimal time-resolution due to the fast diffusion of the ligand into the active site. Ligand diffusion speed into crystals greatly varies depending on several factors: (1) crystal size, (2) mother liquor compositions and (3) nature (chemical and physical properties) of the ligand. Liquid-jet based mixing systems are limited for collecting time points with long time delays (seconds), which are of great relevance to many biological reaction mechanisms. Tape-drive-based approaches are limited for faster time delays (milliseconds regime). The LAMA system overcomes the above limitations and is ideal for conducting mix-and-diffuse time-resolved experiments at synchrotrons in those cases in which the diffusion of a substrate occurs faster than the turnover of the enzymatic reaction.

The LAMA method uses the fix-target device mentioned above, the HARE system, coupled to a piezo-drive droplet generator, which dispenses picoliter-sized droplets containing a substrate onto protein microcrystals and then probed them after a certain time delay. The proof-of-concept experiment was carried out with two model systems, the reaction of lysozyme microcrystals with its natural ligand N-acetyl-chitotriose ((GlcNAc)3) at 50 ms, 100 ms and 1 s time delays [72]. From this experiment, it was seen that the ligand reaches the binding site after 50 ms time delay, achieving a maximum occupancy after 100 ms upon mixing. Apart from the proof-of-concept test, a more "real life" system, the enzyme xylose isomerase and its natural ligand, was chosen [72]. Xylose isomerase is a metal-activated enzyme, and a key component used by bacteria to catalyze the conversion of xylose and glucose into xylulose and fructose, respectively, so that bacteria can use them as nutrients [91]. In this experiment, microcrystals of xylose isomerase were reacted with glucose as substrate and the high-resolution structures of various intermediates were obtained at different time delays (0 ms, 15 ms, 30 ms, 100 ms, 1 s, 4.5 s and 60 s) [72].

The results show that the binding of the glucose molecule occurs within the millisecond time regime, being clearly visible 15 ms after mixing and reaching near full occupancy about 100 ms upon mixing. Then, the glucose ring remains intact until 60 s after mixing, at which the ring is found in its open conformation, an intermediate of this enzyme has never been captured before by other crystallography methods. In previously reported crystal structures, the open ring conformations could only be obtained by soaking or co-crystallization techniques using a linearized (cleaved) glucose [92,93]. Thus, by means of fast diffusion of glucose into the microcrystals it has been possible to capture the first reaction intermediate of the isomerization reaction using the wild-type enzyme with its natural substrate. The initial and final states of the reaction of xylose isomerase with glucose, along with the intermediate states, are shown in Figure 3. This study clearly demonstrates the high applicability of the LAMA method for TR-SSX studies in the millisecond to high seconds time regime. In addition, the LAMA method consumes a significantly less amount of ligand that current mixing devices, making it also ideal for high-throughput drug screening approaches.

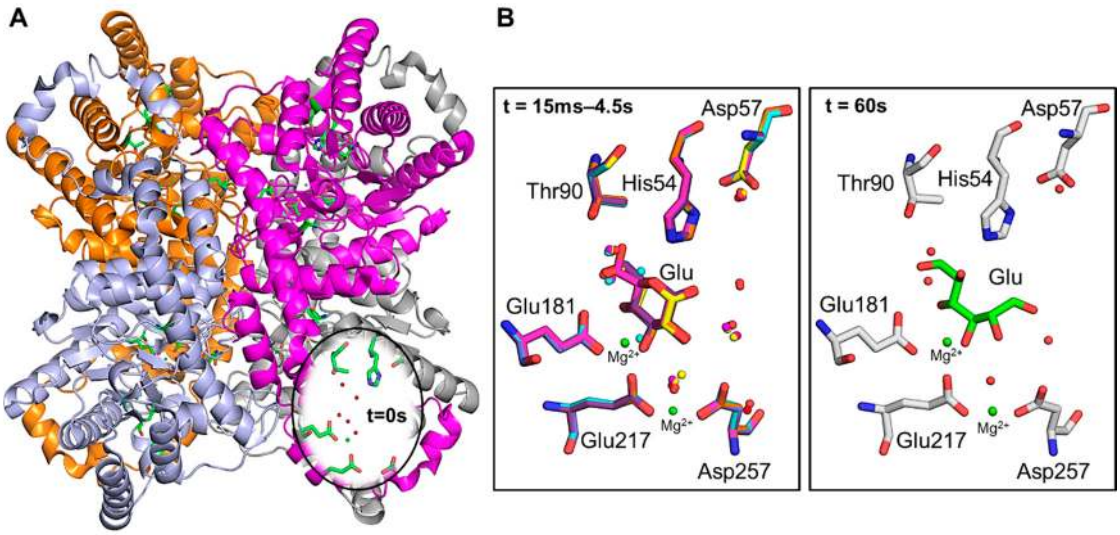

Figure 3. TR-SSX for xylose isomerase with LAMA system. (**A**) Cartoon representation of the tetramer structure of xylose isomerase. The key residues at the catalytic site are highlighted as green sticks. The black circle shows a closer view of the key residues in the resting state (t = 0 s). (**B**) Close-up views of the xylose isomerase active site shown at different time points upon mixing. Left panel shows the superimposition of xylose isomerase structures between t = 15 ms and t = 4.5 ms in complex with glucose in closed ring conformation. Right panel shows the structure of xylose isomerase at t = 60 s with the glucose in open ring conformation. The active site residues and the glucose molecules are shown as sticks, waters as red spheres and magnesium as green spheres.

5.3. TR-SSX with Hybrid Sample Delivery Devices

It is well-known that liquid injectors, such as those used to deliver samples at XFELs, are not suitable for SSX because the jet flow rates are faster than the residency time of the crystals in the interaction region. However, it has been demonstrated that even with liquid injectors, if a T-junction mixing geometry is used, it is possible to carry out mix-and-inject TR-SFX experiments to study protein dynamics at time delays between 500 ms and a few seconds or more [31,33]. With this in mind, Beyerlein and co-workers came up with a novel sample delivery method for conducting time-resolved experiments at synchrotrons [58]. The novel mixing injector combines T-junction mixing and the fixed target approaches [58].

The proof-of-concept of a TR-SSX using the hybrid sample delivery device, commonly known as the tape-drive device, was to explore the binding of a natural short carbohydrate, the (GlcNAc)3, that acts as inhibitor of lysozyme [58]. Lysozyme catalyze the hydrolysis of β-(1,4)-linkages between *N*-acetylmuramic acid (MurNAc) and *N*-acetyl-D-glucosamine (GlcNAc) in peptidoglycans, the cell wall that protects bacteria from the exterior [94]. The binding site of lysozyme can accommodate up to six GlcNAc residues of a chitin polymer, each binding in six subsites along a cleft of the protein. Cleavage occurs at the linkage between the GlcNAc residues occupying the third and fourth subsites [94,95]. In this TR-SSX study, lysozyme microcrystals of less than 10 µm in size were mixed with the natural substrate (GlcNAc)3 using a T-junction mixer and the mixture dispensed onto a polyimide tape, which was continuously rolling from a feeder roller to a collector roll [58]. The speed of the tape was kept constant to 0.6 mm/s, resulting in a translation distance of 24 µm between frames. The flow rate of the two solution was kept constant to 0.6 µL/min to ensure a 1:1 mixing ratio. The mix-and-diffusion SSX experiment was carried out on P11 beamline at PETRA III. X-rays were generated as pulses of 7.5 ms duration at a frequency of 25 Hz by a rotating beam chopper placed upstream of the focusing optics, and this was synchronized with the readout of the detector PILATUS 6M. Two mixing times were tested, 2 and 50 s, by replacing the thickness and the length of the capillaries. Data collection time was 8.5 h for each mixing time, resulting in a total sample consumption of 300 uL (<20 mg of protein). Electron density maps of the data set at 2 s show the ligand chitotriose at the binding site demonstrating that the tape-drive device can be used as an effective

mix-and-diffusion device. At this time delay, more than 90% of the lysozyme binding sites were occupied by the substrate, being nearly to 100% in the case of 50 s time delay. The most significant differences were found in a network of water molecules connecting the substrate to the binding site. They found a higher number of waters at 2 s time delay than at 50 s.

This proof-of-concept experiment opens up the possibility of investigating enzymatic reactions that are on a similar timescale, though further advances in sample delivery methods able to deliver crystals at higher speeds, combined with advances in detector technology along with brighter synchrotron sources and the use of pink X-ray beams could reduce the time scale below 1 s.

5.4. Goniometer-Based Time-Resolved Serial Oscillation Crystallography (TR-SOX)

As it is well-known, SX bases on recording still snapshots from hundred thousand of crystals requiring large amounts of sample. Aumonier and co-workers present an alternative way of collecting data where the sample is subjected to oscillation [74] This method has been called serial oscillation crystallography (SOX). Using SOX one can determine crystal structures from only tens to hundreds of microcrystals, reducing sample consumption notably. As proof-of-concept experiment, Aumonier and co-workers carried out a TR-SOX experiments coupled with "in crystallo" optical spectroscopy to follow and provide dynamics insight into the activation mechanism of the light, oxygen and voltage 2 (LOV2) domain of the phototropin-2 protein from *Arabidosis thaliana* [74]. Phototropin-2 is a plasma membrane-associated photoreceptor of blue light and UV-A/B radiation that mediates phototropism, chloroplast positioning and stomatal opening [96]. Phototropin-2 contain two LOV domains at the protein N-terminus (LOV1 and LOV2) and an additional C-terminal Ser/Thr kinase domain. Both LOV domains are bound with their chromophore, flavin mononucleotide (FMN), which absorbs blue and UV-A/B light [97,98]. The photochemical properties of phototropins-2 rely on the interaction between LOV1 and LOV2, which is facilitated by their intervening linker sequence [96].

The SOX experiments were conducted at room temperature using a humidity control device at beamline ID30A-3 at the ESRF. Crystals ($50 \times 50 \times 50$ μm^3) were mounted on regular goniometer and data collection carried out on an EIGER 4M detector using a 15 um diameter beam size. For each crystal, 990 frames were collected with a 0.5° oscillation and an exposure for about 4.1 s, in some way the LED illumination was synchronized with the X-ray shutter opening, the goniometer axis rotation and the readout of the detector [74]. To prevent crystals from being radiation damaged, the photon flux was attenuated so that the dose absorbed per crystals was always below 170 kGy. The light state of the phototropin-2 was obtained by illuminating a total of 88 crystals with a UV-vis LED at a wavelength of 470 nm. For the dark state, a total of 32 crystals were measured without LED illumination. To build up the light state, data sets of each of the 88 crystals were split into 66 sub-data sets, each containing 15 frames corresponding to a total of 66 time points from 63 ms to 4.1 s. The light absorption by the chromophore FMN leads to conformational changes of the neighboring residues (Val392, Ile403, Cys426, Phe470, Gln489), as well was of the own FMN within the time scale explored in this study (Figure 4). These molecular motions lead to the formation of a covalent bond between Cys426 and the FMN that forces the chromophore to rotate about 6° [74].

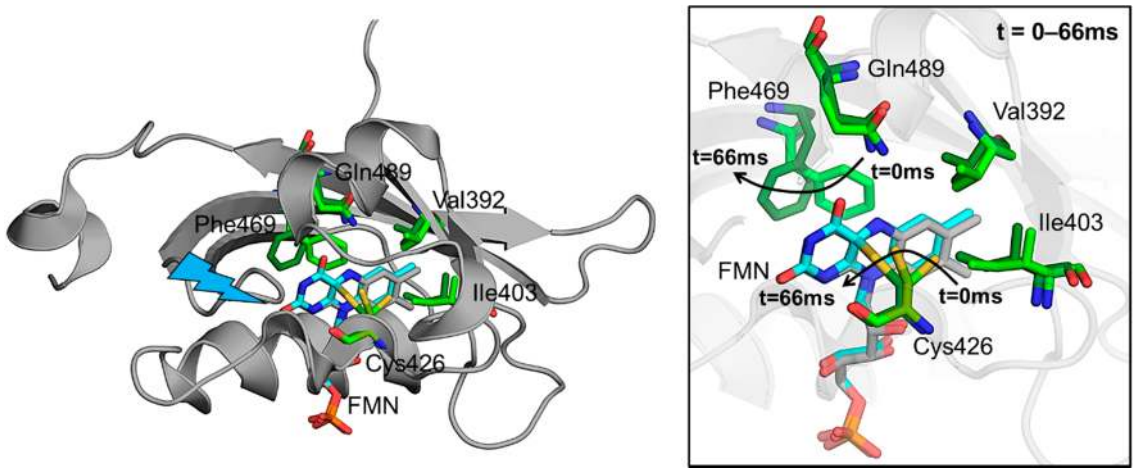

Figure 4. TR-SSX for the LOV2 domain of phototropin-2. (**Left**) Cartoon representation of the LOV2 domain. Key residues and the FMN chromophore at the catalytic site are highlighted as sticks representation. (**Right**) Closer view of catalytic site. The black arrows illustrate the changes occurring at time point 66 ms upon light illumination. Major changes occur for Cys426 and Phe469 (light green represents t = 0 s and dark green t = 66 ms). The FMN chromophore is shown as gray cartoon for t = 0 s and cyan for t = 66 ms.

6. In-Flow Microfluidics Devices for TR-SSX

Despite all of the above sample delivery approaches have shown to produce high-quality SSX and TR-SSX data, they all require the handling and transfer of microcrystal slurries during loading, which sometimes can be problematic samples that are sensitive to changes in environment such as humidity changes and mechanical stress. An alternative is the use of microfluidic devices, which have emerged as platforms for in situ crystallization as well as sample delivery methods at synchrotrons. With microfluidics, one can probe microcrystals in their original mother liquor with no or minimal environment changes. As stated by Alexandra Ros and co-workers [34], essentially, all sample delivery approaches can qualify as microfluidic techniques as the critical dimensions of sample delivery are adapted to the size of the crystals used in serial crystallography experiments, which ranges from a few micrometers to a few tens of micrometers. With that in mind, I will refer to microfluidic devices to all those devices in which the crystal slurries are continuously flowed in micrometer-sized channels, in-flow microfluidic devices.

Since the first in-flow SSX experiment reported by Stellato and co-workers, in which a slurry of lysozyme microcrystals was continuously flowed through a glass capillary [45], no further technical optimizations of in-flow microfluidics followed until very recently. Monteiro et al. have developed in-flow 2D [73] and 3D-printed [75] microfluidic chip devices. The proof-of-concept of collecting SSX data using a flow-focused sample was carried out with a 2D in-flow microfluidic device in which the crystal structure of lysozyme was determined to 2.1 Å resolution using just 30 µL of sample in about 1 h of continuous data collection [73]. The second experiment of flow-focused sample was carried out with a 3D-printed in-flow microfluidic device [75]. The crystal structures of lysozyme and aspartate α-decarboxylase (ADC) proteins were determined with sample consumption similar to that of the 2D device. However, a big advantage of 3D-printed devices over 2D devices is that they reduce the difficulty of the experimental design, as well as simplify chip fabrication significantly. In addition, in-flow microfluidic devices have been demonstrated to avoid clogging issues and operate without interruption for multiple hours. Despite it has yet to be demonstrated, in-flow microfluidics also offers the possibility of future millisecond-mixing-based time-resolved structural experiments at modern synchrotrons in which ligands (substrates or antibiotics) can be added to the focusing buffer to trigger a reaction mechanism “in crystallo”.

7. Conclusions

The SSX methods emerged as a complementary method to standard crystallography, and will continue evolving in upcoming years. However, current existing methods are mature enough for routine use. The SSX approach overcomes the limitations of standard crystallography with single-crystals with respect to the availability of large crystals, crystal handling, cryo-cooling and the radiation damage that a single crystal can tolerate. In standard crystallography, single crystals must be harvested and mounted, one at a time, followed by X-ray diffraction screening, which makes the screening of all available crystals impractical. As reviewed here, SSX offers attractive alternatives with innovative and automated sample delivery and serial data collection methods. The technologies developed for SSX along with the next generation synchrotron sources will enable the possibility of acquiring better data from smaller crystals, which was either impossible or rather tedious and time consuming previously. It should be feasible to obtain high resolution structures with micrometer or even nanometer sized crystals. The serial nature of the SSX experiment makes automation indispensable, which calls for further development in workflows from crystallization, sample delivery to data collection, processing and merging. SSX is also important for screening initial hits in crystallization and for pre-characterizing samples for SFX experiments.

Time resolved crystallography (TRX) is a powerful tool for understanding protein dynamics and catalysis, allowing much greater understanding of structural dynamics and intermediate states in proteins. Early TRX work was largely limited to proteins whose conformational changes could be triggered optically using an intrinsic chromophore, and whose motions were reversible in the crystal, so that a single crystal could be pumped and reset multiple times to generate the diffraction data. These classical approaches of TRX via populating intermediate states by protein mutations or chemical trapping, gradually fell out of favor in the past decade. However, the recent development of serial crystallography (SX) at XFELs [99], coupled with advances in sample delivery methods [100] and X-ray detectors technology [101–105], has resulted in a renewed interest in TRX, first at free-electron lasers (TR-SFX) (see review [37]) and more recently at synchrotron sources (TR-SSX) (see Table 1).

As discussed in this review, TR experiments, including those of irreversible reactions, similar to TR-SFX, can also be performed at synchrotrons, albeit with lower time resolution. Despite, time-resolved experiments at synchrotron beamlines are limited to a time resolution of several milliseconds, the time needed to collect diffraction patterns with sufficient intensity. However, upcoming synchrotron upgrades to next-generation diffraction-limited sources will allow measurements in the microsecond and perhaps nanosecond range, which is highly relevant for the study of the majority of enzymatic processes in biology. As well, to further increase the photon flux (∼100 times) and the time resolution, a pink X-ray beam can be used instead of a monochromatic beam. This also works in the high-throughput serial data-collection regime, as successfully demonstrated by raster scanning a fixed target [57] and viscous jets [70].

Funding: This work was supported by the "Ayuda de Atracción y Retención de Talento Investigador" from the Community of Madrid, Spain (REF: 2019-T1BMD-15552).

Acknowledgments: J.M.M.-G. thanks Jose A. Gavira for his careful reading and commenting on this article.

Conflicts of Interest: The author declares no conflict of interest.

References

1. Blake, C.; Koenig, D.; Mair, G.; North, A.; Phillips, D.; Sarma, V. The three-dimensional structure of hen eggwhite lysozyme. *Nature* **1965**, *206*, 757–761. [CrossRef] [PubMed]
2. Van Den Bedem, H.; Fraser, J.S. Integrative, dynamic structural biology at atomic resolution—It's about time. *Nat. Methods* **2015**, *12*, 307–318. [CrossRef] [PubMed]
3. Hajdu, J.; Johnson, L.N. Progress with Laue Diffraction Studies on Protein and Virus Crystals. *Biochemistry* **1990**, *29*, 1669–1678. [CrossRef]

4. Bourgeois, D.; Ursby, T.; Wulff, M.; Pradervand, C.; Legrand, A.; Schildkamp, W.; Labouré, S.; Srajer, V.; Teng, T.Y.; Roth, M.; et al. Feasibility and realization of single-pulse Laue diffraction on macromolecular crystals at ESRF. *J. Synchrotron. Radiat.* **1996**, *3*, 65–74. [CrossRef]
5. Genick, U.K.; Borgstahl, G.E.O.; Ng, K.; Ren, Z.; Pradervand, C.; Burke, P.M.; Šrajer, V.; Teng, T.Y.; Schildkamp, W.; McRee, D.E.; et al. Structure of a protein photocycle intermediate by millisecond time- resolved crystallography. *Science* **1997**, *275*, 1471–1475. [CrossRef] [PubMed]
6. Ihee, H.; Rajagopal, S.; Srajer, V.; Pahl, R.; Anderson, S.; Schmidt, M.; Schotte, F.; Anfinrud, P.A.; Wulff, M.; Moffat, K. Visualizing reaction pathways in photoactive yellow protein from nanoseconds to seconds. *Proc. Natl. Acad. Sci. USA* **2005**, *102*, 7145–7150. [CrossRef]
7. Knapp, J.E.; Pahl, R.; Šrajer, V.; Royer, W.E. Allosteric action in real time: Time-resolved crystallographic studies of a cooperative dimeric hemoglobin. *Proc. Natl. Acad. Sci. USA* **2006**, *103*, 7649–7654. [CrossRef] [PubMed]
8. Moffat, K.; Szebenyi, B.D. X-ray Laue Diffraction from Protein Crystals. *Science* **1984**, *223*, 1423–1425. [CrossRef] [PubMed]
9. Ren, Z.; Šrajer, V.; Knapp, J.E.; Royer, W.E. Cooperative macromolecular device revealed by meta-analysis of static and time-resolved structures. *Proc. Natl. Acad. Sci. USA* **2012**, *109*, 107–112. [CrossRef]
10. Schmidt, M.; Nienhaus, K.; Pahl, R.; Krasselt, A.; Anderson, S.; Parak, F.; Nienhaus, G.U.; Šrajer, V. Ligand migration pathway and protein dynamics in myoglobin: A time-resolved crystallographic study on L29W MbCO. *Proc. Natl. Acad. Sci. USA* **2005**, *102*, 11704–11709. [CrossRef]
11. Schmidt, M.; Graber, T.; Henning, R.; Srajer, V. Five-dimensional crystallography. *Acta Crystallogr. Sect. A Found. Crystallogr.* **2010**, *66*, 198–206. [CrossRef]
12. Bourgeois, D.; Royant, A. Advances in kinetic protein crystallography. *Curr. Opin. Struct. Biol.* **2005**, *15*, 538–547. [CrossRef] [PubMed]
13. Neutze, R.; Moffat, K. Time-resolved structural studies at synchrotrons and X-ray free electron lasers: Opportunities and challenges. *Curr. Opin. Struct. Biol.* **2012**, *22*, 651–659. [CrossRef] [PubMed]
14. Šrajer, V.; Schmidt, M. Watching proteins function with time-resolved x-ray crystallography. *J. Phys. D Appl. Phys.* **2017**, *50*, 373001. [CrossRef] [PubMed]
15. Stoddard, B.L. Trapping reaction intermediates in macromolecular crystals for structural analyses. *Methods* **2001**, *24*, 125–138. [CrossRef] [PubMed]
16. Schotte, F.; Lim, M.; Jackson, T.A.; Smirnov, A.V.; Soman, J.; Olson, J.S.; Phillips, G.N.; Wulff, M.; Anfinrud, P.A. Watching a protein as it functions with 150-ps time-resolved x-ray crystallography. *Science* **2003**, *300*, 1944–1947. [CrossRef] [PubMed]
17. Schotte, F.; Cho, H.S.; Kaila, V.R.I.; Kamikubo, H.; Dashdorj, N.; Henry, E.R.; Graber, T.J.; Henning, R.; Wulff, M.; Hummer, G.; et al. Watching a signaling protein function in real time via 100-ps time-resolved Laue crystallography. *Proc. Natl. Acad. Sci. USA* **2012**, *109*, 19256–19261. [CrossRef]
18. Jung, Y.O.; Lee, J.H.; Kim, J.; Schmidt, M.; Moffat, K.; Šrajer, V.; Ihee, H. Volume-conserving trans-cis isomerization pathways in photoactive yellow protein visualized by picosecond X-ray crystallography. *Nat. Chem.* **2013**, *5*, 212–220. [CrossRef]
19. Tenboer, J.; Basu, S.; Zatsepin, N.; Pande, K.; Milathianaki, D.; Frank, M.; Hunter, M.; Boutet, S.; Williams, G.J.; Koglin, J.E.; et al. Time-resolved serial crystallography captures high-resolution intermediates of photoactive yellow protein. *Science* **2014**, *346*, 1242–1246. [CrossRef]
20. Pande, K.; Hutchison, C.D.M.; Groenhof, G.; Aquila, A.; Robinson, J.S.; Tenboer, J.; Basu, S.; Boutet, S.; DePonte, D.P.; Liang, M.; et al. Femtosecond structural dynamics drives the trans/cis isomerization in photoactive yellow protein. *Science* **2016**, *352*, 725–729. [CrossRef]
21. Kupitz, C.; Basu, S.; Grotjohann, I.; Fromme, R.; Zatsepin, N.A.; Rendek, K.N.; Hunter, M.S.; Shoeman, R.L.; White, T.A.; Wang, D.; et al. Serial time-resolved crystallography of photosystem II using a femtosecond X-ray laser. *Nature* **2014**, *513*, 261–265. [CrossRef]
22. Kern, J.; Tran, R.; Alonso-Mori, R.; Koroidov, S.; Echols, N.; Hattne, J.; Ibrahim, M.; Gul, S.; Laksmono, H.; Sierra, R.G.; et al. Taking snapshots of photosynthetic water oxidation using femtosecond X-ray diffraction and spectroscopy. *Nat. Commun.* **2014**, *5*, 1–11. [CrossRef] [PubMed]
23. Kern, J.; Chatterjee, R.; Young, I.D.; Fuller, F.D.; Lassalle, L.; Ibrahim, M.; Gul, S.; Fransson, T.; Brewster, A.S.; Alonso-Mori, R.; et al. Structures of the intermediates of Kok's photosynthetic water oxidation clock. *Nature* **2018**, *563*, 421–425. [CrossRef]
24. Suga, M.; Akita, F.; Sugahara, M.; Kubo, M.; Nakajima, Y.; Nakane, T.; Yamashita, K.; Umena, Y.; Nakabayashi, M.; Yamane, T.; et al. Light-induced structural changes and the site of O=O bond formation in PSII caught by XFEL. *Nature* **2017**, *543*, 131–135. [CrossRef] [PubMed]
25. Suga, M.; Akita, F.; Yamashita, K.; Nakajima, Y.; Ueno, G.; Li, H.; Yamane, T.; Hirata, K.; Umena, Y.; Yonekura, S.; et al. An oxyl/oxo mechanism for oxygen-oxygen coupling in PSII revealed by an x-ray free-electron laser. *Science* **2019**, *366*, 334–338. [CrossRef]
26. Young, I.D.; Ibrahim, M.; Chatterjee, R.; Gul, S.; Fuller, F.; Koroidov, S.; Brewster, A.S.; Tran, R.; Alonso-Mori, R.; Kroll, T.; et al. No TiStructure of photosystem II and substrate binding at room temperaturetle. *Nature* **2016**, *540*, 453–457. [CrossRef]
27. Nango, E.; Royant, A.; Kubo, M.; Nakane, T.; Wickstrand, C.; Kimura, T.; Tanaka, T.; Tono, K.; Song, C.; Tanaka, R.; et al. A three-dimensional movie of structural changes in bacteriorhodopsin. *Science* **2016**, *354*, 1552–1557. [CrossRef]

28. Nogly, P.; Weinert, T.; James, D.; Carbajo, S.; Ozerov, D.; Furrer, A.; Gashi, D.; Borin, V.; Skopintsev, P.; Jaeger, K.; et al. Retinal isomerization in bacteriorhodopsin captured by a femtosecond x-ray laser. *Science* **2018**, *361*, eaat0094. [CrossRef] [PubMed]
29. Weinert, T.; Skopintsev, P.; James, D.; Dworkowski, F.; Panepucci, E.; Kekilli, D.; Furrer, A.; Brünle, S.; Mous, S.; Ozerov, D.; et al. Proton uptake mechanism in bacteriorhodopsin captured by serial synchrotron crystallography. *Science* **2019**, *365*, 61–65. [CrossRef] [PubMed]
30. Moffat, K. Laue diffraction. *Methods Enzym.* **1997**, *277*, 433–447.
31. Kupitz, C.; Olmos, J.L.; Holl, M.; Tremblay, L.; Pande, L.; Pandey, S.; Oberthür, D.; Hunter, M.; Liang, M.; Aquila, A.; et al. Structural enzymology using X-ray free electron lasers. *Struct. Dyn.* **2017**, *4*, 044003. [CrossRef]
32. Olmos, J.L.; Pandey, S.; Martin-Garcia, J.M.; Calvey, G.; Katz, A.; Knoska, J.; Kupitz, C.; Hunter, M.S.; Liang, M.; Oberthuer, D.; et al. Enzyme intermediates captured "on the fly" by mix-and-inject serial crystallography. *BMC Biol.* **2018**, *16*, 1–15. [CrossRef] [PubMed]
33. Stagno, J.R.; Liu, Y.; Bhandari, Y.R.; Conrad, C.E.; Panja, S.; Swain, M.; Fan, L.; Nelson, G.; Li, C.; Wendel, D.R.; et al. Structures of riboswitch RNA reaction states by mix-and-inject XFEL serial crystallography. *Nature* **2017**, *541*, 242–246. [CrossRef] [PubMed]
34. Echelmeier, A.; Sonker, M.; Ros, A. Microfluidic sample delivery for serial crystallography using XFELs. *Anal. Bioanal. Chem.* **2019**, *411*, 6535–6547. [CrossRef]
35. Botha, S.; Nass, K.; Barends, T.R.M.; Kabsch, W.; Latz, B.; Dworkowski, F.; Foucar, L.; Panepucci, E.; Wang, M.; Shoeman, R.L.; et al. Room-temperature serial crystallography at synchrotron X-ray sources using slowly flowing free-standing high-viscosity microstreams. *Acta Crystallogr. Sect. D Biol. Crystallogr.* **2015**, *71*, 387–397. [CrossRef] [PubMed]
36. Nogly, P.; James, D.; Wang, D.; White, T.A.; Zatsepin, N.; Shilova, A.; Nelson, G.; Liu, H.; Johansson, L.; Heymann, M.; et al. Lipidic cubic phase serial millisecond crystallography using synchrotron radiation. *IUCrJ* **2015**, *2*, 168–176. [CrossRef] [PubMed]
37. Fromme, P.; Graves, W.S.; Martin-Garcia, J.M. Serial Femtosecond Crystallography: A Decade at the Forefront in Structural Biology. *eLS* **2020**, 1–17. [CrossRef]
38. Martin-Garcia, J.M.; Conrad, C.E.; Coe, J.; Roy-Chowdhury, S.; Fromme, P. Serial femtosecond crystallography: A revolution in structural biology. *Arch. Biochem. Biophys.* **2016**, *602*, 32–47. [CrossRef]
39. Kirian, R.A.; White, T.A.; Holton, J.M.; Chapman, H.N.; Fromme, P.; Barty, A.; Lomb, L.; Aquila, A.; Maia, F.R.N.C.; Martin, A.V.; et al. Structure-factor analysis of femtosecond microdiffraction patterns from protein nanocrystals. *Acta Crystallogr. Sect. A Found. Crystallogr.* **2011**, *67*, 131–140. [CrossRef]
40. Kirian, R.A.; Wang, X.; Weierstall, U.; Schmidt, K.E.; Spence, J.C.H.; Hunter, M.; Fromme, P.; White, T.; Chapman, H.N.; Holton, J. Femtosecond protein nanocrystallography—data analysis methods. *Opt. Express* **2010**, *18*, 5713. [CrossRef] [PubMed]
41. Barty, A.; Kirian, R.A.; Maia, F.R.N.C.; Hantke, M.; Yoon, C.H.; White, T.A.; Chapman, H. *Cheetah*: Software for high-throughput reduction and analysis of serial femtosecond X-ray diffraction data. *J. Appl. Crystallogr.* **2014**, *47*, 1118–1131. [CrossRef]
42. White, T.A.; Mariani, V.; Brehm, W.; Yefanov, O.; Barty, A.; Beyerlein, K.R.; Chervinskii, F.; Galli, L.; Gati, C.; Nakane, T.; et al. Recent developments in *CrystFEL*. *J. Appl. Crystallogr.* **2016**, *49*, 680–689. [CrossRef]
43. Mariani, V.; Morgan, A.; Yoon, C.H.; Lane, T.J.; White, T.A.; O'Grady, C.; Kuhn, M.; Aplin, S.; Koglin, J.; Barty, A.; et al. *OnDA*: Online data analysis and feedback for serial X-ray imaging. *J. Appl. Crystallogr.* **2016**, *49*, 1073–1080. [CrossRef] [PubMed]
44. Gati, C.; Bourenkov, G.; Klinge, M.; Rehders, D.; Stellato, F.; Oberthür, D.; Yefanov, O.; Sommer, B.P.; Mogk, S.; Duszenko, M.; et al. Serial crystallography on in vivo grown microcrystals using synchrotron radiation. *IUCrJ* **2014**, *1*, 87–94. [CrossRef] [PubMed]
45. Stellato, F.; Oberthür, D.; Liang, M.; Bean, R.; Gati, C.; Yefanov, O.; Barty, A.; Burkhardt, A.; Fischer, P.; Galli, L.; et al. Room-temperature macromolecular serial crystallography using synchrotron radiation. *IUCrJ* **2014**, *1*, 204–212. [CrossRef]
46. Heymann, M.; Opthalage, A.; Wierman, J.L.; Akella, S.; Szebenyi, D.M.E.; Gruner, S.M.; Fraden, S. Room-temperature serial crystallography using a kinetically optimized microfluidic device for protein crystallization and on-chip X-ray diffraction. *IUCrJ* **2014**, *1*, 349–360. [CrossRef] [PubMed]
47. Coquelle, N.; Brewster, A.S.; Kapp, U.; Shilova, A.; Weinhausen, B.; Burghammer, M.; Colletier, J.-P. Raster-scanning serial protein crystallography using micro- and nano-focused synchrotron beams. *Acta Crystallogr. Sect. D Biol. Crystallogr.* **2015**, *71*, 1184–1196. [CrossRef]
48. Murray, T.D.; Lyubimov, A.Y.; Ogata, C.M.; Vo, H.; Uervirojnangkoorn, M.; Brunger, A.T.; Berger, J.M. A high-transparency, micro-patternable chip for X-ray diffraction analysis of microcrystals under native growth conditions. *Acta Crystallogr. Sect. D Biol. Crystallogr.* **2015**, *71*, 1987–1997. [CrossRef] [PubMed]
49. Huang, C.-Y.; Olieric, V.; Ma, P.; Panepucci, E.; Diederichs, K.; Wang, M.; Caffrey, M. *In meso* in situ serial X-ray crystallography of soluble and membrane proteins. *Acta Crystallogr. Sect. D Biol. Crystallogr.* **2015**, *71*, 1238–1256. [CrossRef] [PubMed]
50. Zander, U.; Bourenkov, G.; Popov, A.N.; de Sanctis, D.; Svensson, O.; McCarthy, A.A.; Round, E.; Gordeliy, V.; Mueller-Dieckmann, C.; Leonard, G.A. *MeshAndCollect*: An automated multi-crystal data-collection workflow for synchrotron macromolecular crystallography beamlines. *Acta Crystallogr. Sect. D Biol. Crystallogr.* **2015**, *71*, 2328–2343. [CrossRef]
51. Mueller, C.; Marx, A.; Epp, S.W.; Zhong, Y.; Kuo, A.; Balo, A.R.; Soman, J.; Schotte, F.; Lemke, H.T.; Owen, R.L.; et al. Fixed target matrix for femtosecond time-resolved and in situ serial micro-crystallography. *Struct. Dyn.* **2015**, *2*, 54302. [CrossRef]
52. Roedig, P.; Vartiainen, I.; Duman, R.; Panneerselvam, S.; Stübe, N.; Lorbeer, O.; Warmer, M.; Sutton, G.; Stuart, D.I.; Weckert, E.; et al. A micro-patterned silicon chip as sample holder for macromolecular crystallography experiments with minimal background scattering. *Sci. Rep.* **2015**, *5*, 10451. [CrossRef] [PubMed]

53. Huang, C.-Y.; Olieric, V.; Ma, P.; Howe, N.; Vogeley, L.; Liu, X.; Warshamanage, R.; Weinert, T.; Panepucci, E.; Kobilka, B.; et al. *In meso* in situ serial X-ray crystallography of soluble and membrane proteins at cryogenic temperatures. *Acta Crystallogr. Sect. D Struct. Biol.* **2016**, *72*, 93–112. [CrossRef]
54. Roedig, P.; Duman, R.; Sanchez-Weatherby, J.; Vartiainen, I.; Burkhardt, A.; Warmer, M.; David, C.; Wagner, A.; Meents, A. Room-temperature macromolecular crystallography using a micro-patterned silicon chip with minimal background scattering. *J. Appl. Crystallogr.* **2016**, *49*, 968–975. [CrossRef] [PubMed]
55. Hasegawa, K.; Yamashita, K.; Murai, T.; Nuemket, N.; Hirata, K.; Ueno, G.; Ago, H.; Nakatsu, T.; Kumasaka, T.; Yamamoto, M. Development of a dose-limiting data collection strategy for serial synchrotron rotation crystallography. *J. Synchrotron. Radiat.* **2017**, *24*, 29–41. [CrossRef] [PubMed]
56. Martin-Garcia, J.M.; Conrad, C.E.; Nelson, G.; Stander, N.; Zatsepin, N.A.; Zook, J.; Zhu, L.; Geiger, J.; Chun, E.; Kissick, D.; et al. Serial millisecond crystallography of membrane and soluble protein microcrystals using synchrotron radiation. *IUCrJ* **2017**, *4*, 439–454. [CrossRef]
57. Meents, A.; Wiedorn, M.O.; Srajer, V.; Henning, R.; Sarrou, I.; Bergtholdt, J.; Barthelmess, M.; Reinke, P.Y.A.; Dierksmeyer, D.; Tolstikova, A.; et al. Pink-beam serial crystallography. *Nat. Commun.* **2017**, *8*, 1281. [CrossRef]
58. Beyerlein, K.R.; Dierksmeyer, D.; Mariani, V.; Kuhn, M.; Sarrou, I.; Ottaviano, A.; Awel, S.; Knoska, J.; Fuglerud, S.; Jönsson, O.; et al. Mix-and-diffuse serial synchrotron crystallography. *IUCrJ* **2017**, *4*, 769–777. [CrossRef] [PubMed]
59. Weinert, T.; Olieric, N.; Cheng, R.; Brünle, S.; James, D.; Ozerov, D.; Gashi, D.; Vera, L.; Marsh, M.; Jaeger, K.; et al. Serial millisecond crystallography for routine room-temperature structure determination at synchrotrons. *Nat. Commun.* **2017**, *8*, 542. [CrossRef]
60. Kovácsová, G.; Grünbein, M.L.; Kloos, M.; Barends, T.R.M.; Schlesinger, R.; Heberle, J.; Kabsch, W.; Shoeman, R.L.; Doak, R.B.; Schlichting, I. Viscous hydrophilic injection matrices for serial crystallography. *IUCrJ* **2017**, *4*, 400–410. [CrossRef]
61. Boudes, M.; Garriga, D.; Fryga, A.; Caradoc-Davies, T.; Coulibaly, F. A pipeline for structure determination of in vivo -grown crystals using *in cellulo* diffraction. *Acta Crystallogr. Sect. D Struct. Biol.* **2016**, *72*, 576–585. [CrossRef]
62. Foos, N.; Seuring, C.; Schubert, R.; Burkhardt, A.; Svensson, O.; Meents, A.; Chapman, H.N.; Nanao, M.H. X-ray and UV radiation-damage-induced phasing using synchrotron serial crystallography. *Acta Crystallogr. Sect. D Struct. Biol.* **2018**, *74*, 366–378. [CrossRef] [PubMed]
63. Botha, S.; Baitan, D.; Jungnickel, K.E.J.; Oberthür, D.; Schmidt, C.; Stern, S.; Wiedorn, M.O.; Perbandt, M.; Chapman, H.N.; Betzel, C. *De novo* protein structure determination by heavy-atom soaking in lipidic cubic phase and SIRAS phasing using serial synchrotron crystallography. *IUCrJ* **2018**, *5*, 524–530. [CrossRef] [PubMed]
64. Gao, Y.; Xu, W.; Shi, W.; Soares, A.; Jakoncic, J.; Myers, S.; Martins, B.; Skinner, J.; Liu, Q.; Bernstein, H.; et al. High-speed raster-scanning synchrotron serial microcrystallography with a high-precision piezo-scanner. *J. Synchrotron. Radiat.* **2018**, *25*, 1362–1370. [CrossRef]
65. Guo, G.; Fuchs, M.R.; Shi, W.; Skinner, J.; Berman, E.; Ogata, C.M.; Hendrickson, W.A.; McSweeney, S.; Liu, Q. Sample manipulation and data assembly for robust microcrystal synchrotron crystallography. *IUCrJ* **2018**, *5*, 238–246. [CrossRef]
66. Gicquel, Y.; Schubert, R.; Kapis, S.; Bourenkov, G.; Schneider, T.; Perbandt, M.; Betzel, C.; Chapman, H.N.; Heymann, M. Microfluidic Chips for In Situ Crystal X-ray Diffraction and In Situ Dynamic Light Scattering for Serial Crystallography. *J. Vis. Exp.* **2018**, 57133. [CrossRef]
67. Ren, Z.; Ayhan, M.; Bandara, S.; Bowatte, K.; Kumarapperuma, I.; Gunawardana, S.; Shin, H.; Wang, C.; Zeng, X.; Yang, X. Crystal-on-crystal chips for in situ serial diffraction at room temperature. *Lab Chip.* **2018**, *18*, 2246–2256. [CrossRef] [PubMed]
68. Schulz, E.C.; Mehrabi, P.; Müller-Werkmeister, H.M.; Tellkamp, F.; Jha, A.; Stuart, W.; Persch, E.; De Gasparo, R.; Diederich, F.; Pai, E.F.; et al. The hit-and-return system enables efficient time-resolved serial synchrotron crystallography. *Nat. Methods* **2018**, *15*, 901–904. [CrossRef]
69. Basu, S.; Kaminski, J.W.; Panepucci, E.; Huang, C.-Y.; Warshamanage, R.; Wang, M.; Wojdyla, J.A. Automated data collection and real-time data analysis suite for serial synchrotron crystallography. *J. Synchrotron. Radiat.* **2019**, *26*, 244–252. [CrossRef]
70. Martin-Garcia, J.M.; Zhu, L.; Mendez, D.; Lee, M.-Y.; Chun, E.; Li, C.; Hu, H.; Subramanian, G.; Kissick, D.; Ogata, C.; et al. High-viscosity injector-based pink-beam serial crystallography of microcrystals at a synchrotron radiation source. *IUCrJ* **2019**, *6*, 412–425. [CrossRef]
71. Mehrabi, P.; Schulz, E.C.; Agthe, M.; Horrell, S.; Bourenkov, G.; von Stetten, D.; Leimkohl, J.-P.; Schikora, H.; Schneider, T.R.; Pearson, A.R.; et al. Liquid application method for time-resolved analyses by serial synchrotron crystallography. *Nat. Methods* **2019**, *16*, 979–982. [CrossRef]
72. Mehrabi, P.; Schulz, E.C.; Dsouza, R.; Müller-Werkmeister, H.M.; Tellkamp, F.; Miller, R.J.D.; Pai, E.F. Time-resolved crystallography reveals allosteric communication aligned with molecular breathing. *Science* **2019**, *365*, 1167–1170. [CrossRef]
73. Monteiro, D.C.F.; Vakili, M.; Harich, J.; Sztucki, M.; Meier, S.M.; Horrell, S.; Josts, I.; Trebbin, M. A microfluidic flow-focusing device for low sample consumption serial synchrotron crystallography experiments in liquid flow. *J. Synchrotron. Radiat.* **2019**, *26*, 406–412. [CrossRef] [PubMed]
74. Aumonier, S.; Santoni, G.; Gotthard, G.; Von Stetten, D.; Leonard, G.A.; Royant, A. Millisecond time-resolved serial oscillation crystallography of a blue-light photoreceptor at a synchrotron. *IUCrJ* **2020**, *7*, 728–736. [CrossRef]

75. Monteiro, D.C.F.; von Stetten, D.; Stohrer, C.; Sans, M.; Pearson, A.R.; Santoni, G.; van der Linden, P.; Trebbin, M. 3D-MiXD: 3D-printed X-ray-compatible microfluidic devices for rapid, low-consumption serial synchrotron crystallography data collection in flow. *IUCrJ* **2020**, *7*, 207–219. [CrossRef] [PubMed]
76. Zhao, F.Z.; Sun, B.; Yu, L.; Xiao, Q.J.; Wang, Z.J.; Chen, L.L.; Liang, H.; Wang, Q.S.; He, J.H.; Yin, D.C. A novel sample delivery system based on circular motion for: In situ serial synchrotron crystallography. *Lab Chip.* **2020**, *20*, 3888–3898. [CrossRef] [PubMed]
77. de la Mora, E.; Coquelle, N.; Bury, C.S.; Rosenthal, M.; Holton, J.M.; Carmichael, I.; Garman, E.F.; Burghammer, M.; Colletier, J.-P.; Weik, M. Radiation damage and dose limits in serial synchrotron crystallography at cryo- and room temperatures. *Proc. Natl. Acad. Sci. USA* **2020**, *117*, 4142–4151. [CrossRef]
78. Kovalev, K.; Astashkin, R.; Gushchin, I.; Orekhov, P.; Volkov, D.; Zinovev, E.; Marin, E.; Rulev, M.; Alekseev, A.; Royant, A.; et al. Molecular mechanism of light-driven sodium pumping. *Nat. Commun.* **2020**, *11*, 1–11. [CrossRef]
79. Shahsavar, A.; Stohler, P.; Bourenkov, G.; Zimmermann, I.; Siegrist, M.; Guba, W.; Pinard, E.; Sinning, S.; Seeger, M.A.; Schneider, T.R.; et al. Structural insights into the inhibition of glycine reuptake. *Nature* **2021**, *591*, 677–681. [CrossRef]
80. Hasegawa, K.; Baba, S.; Kawamura, T.; Yamamotob, M.; Kumasakaa, T. Evaluation of the data-collection strategy for room-Temperature micro-crystallography studied by serial synchrotron rotation crystallography combined with the humid air and glue-coating method. *Acta Crystallogr. Sect. D Struct. Biol.* **2021**, *77*, 300–312. [CrossRef]
81. Mehrabi, P.; Bücker, R.; Bourenkov, G.; Ginn, H.M.; von Stetten, D.; Müller-Werkmeister, H.M.; Kuo, A.; Morizumi, T.; Eger, B.T.; Ou, W.L.; et al. Serial femtosecond and serial synchrotron crystallography can yield data of equivalent quality: A systematic comparison. *Sci. Adv.* **2021**, *7*, 1–10. [CrossRef] [PubMed]
82. Bolduc, J.M.; Dyer, D.H.; Scott, W.G.; Singer, P.; Sweet, R.M.; Jr, D.E.K.; Stoddard, B.L.; Lyon, S.; Bolduc, J.M.; Dyer, D.H.; et al. Mutagenesis and Laue Structures of Enzyme Intermediates: Isocitrate Dehydrogenase Published by: American Association for the Advancement of Science Mutagenesis and Laue Structures of Enzyme Intermediates: Isocitrate Dehydrogenase. *Science* **2021**, *268*, 1312–1318. [CrossRef] [PubMed]
83. Stoddard, B.L.; Farber, G.K. Direct measurement of reactivity in the protein crystal. *Structure* **1995**, *3*, 991–996. [CrossRef]
84. Helliwell, J.R.; Nieh, Y.P.; Habash, J.; Faulder, P.F.; Raftery, J.; Cianci, M.; Wulff, M.; Hädener, A. Time-resolved and static-ensemble structural chemistry of hydroxymethylbilane synthase. *Faraday Discuss* **2002**, *122*, 131–144. [CrossRef] [PubMed]
85. Ursby, T.; Weik, M.; Fioravanti, E.; Delarue, M.; Goeldner, M.; Bourgeois, D. Cryophotolysis of caged compounds: A technique for trapping intermediate states in protein crystals. *Acta Crystallogr. Sect. D Biol. Crystallogr.* **2002**, *58*, 607–614. [CrossRef]
86. Stoddard, B.L.; Cohen, B.E.; Brubaker, M.; Mesecar, A.D.; Koshland, D.E. Millisecond laue structures of an enzyme-product complex using photocaged substrate analogs. *Nat. Struct. Biol.* **1998**, *5*, 891–897. [CrossRef]
87. Schlichting, I.; Rapp, G.; John, J.; Wittinghofer, A.; Pai, E.F.; Goody, R.S. Biochemical and crystallographic characterization of a complex of c-Ha-ras p21 and caged GTP with flash photolysis. *Proc. Natl. Acad. Sci. USA* **1989**, *86*, 7687–7690. [CrossRef]
88. Schmidt, M. Mix and Inject: Reaction Initiation by Diffusion for Time-Resolved Macromolecular Crystallography. *Adv. Condens. Matter Phys.* **2013**, *2013*, 1–10. [CrossRef]
89. Weierstall, U.; James, D.; Wang, C.; White, T.A.; Wang, D.; Liu, W.; Spence, J.C.H.; Bruce Doak, R.; Nelson, G.; Fromme, P.; et al. Lipidic cubic phase injector facilitates membrane protein serial femtosecond crystallography. *Nat. Commun.* **2014**, *5*, 3309. [CrossRef]
90. Ishigami, I.; Lewis-Ballester, A.; Echelmeier, A.; Brehm, G.; Zatsepin, N.A.; Grant, T.D.; Coe, J.D.; Lisova, S.; Nelson, G.; Zhang, S.; et al. Snapshot of an oxygen intermediate in the catalytic reaction of cytochrome *c* oxidase. *Proc. Natl. Acad. Sci. USA* **2019**, *116*, 3572–3577. [CrossRef]
91. Singh, P.; Kumar, S. Microbial enzyme in food biotechnology. *Enzym. Food Biotechnol. Prod. Appl. Futur. Prospect.* **2018**, 19–28. [CrossRef]
92. Lavie, A.; Allen, K.N.; Petsko, G.A.; Ringe, D. X-ray Crystallographic Structures of d-Xylose Isomerase-Substrate Complexes Position the Substrate and Provide Evidence for Metal Movement during Catalysis. *Biochemistry* **1994**, *33*, 5469–5480. [CrossRef]
93. Kovalevsky, A.; Fisher, Z.; Johnson, H.; Mustyakimov, M.; Waltman, M.J.; Langan, P. Macromolecular neutron crystallography at the Protein Crystallography Station (PCS). *Acta Crystallogr. Sect. D Biol. Crystallogr.* **2010**, *66*, 1206–1212. [CrossRef] [PubMed]
94. Blake, C.C.F.; Johnson, L.N.; Mair, G.A.; North, A.C.T.; Phillips, D.C.; Sarma, V.R. Crystallographic studies of the activity of hen egg-white lysozyme. *Proc. R. Soc. L B Biol. Sci.* **1967**, *167*, 378–388.
95. Vocadlo, D.J.; Davies, G.J.; Laine, R.; Withers, S.G. Catalysis by hen egg-white lysozyme proceeds via a covalent intermediate. *Nature* **2001**, *412*, 835–838. [CrossRef] [PubMed]
96. Kaiserli, E.; Sullivan, S.; Jones, M.A.; Feeney, K.A.; Christie, J.M. Domain swapping to assess the mechanistic basis of Arabidopsis phototropin 1 receptor kinase activation and endocytosis by blue light. *Plant. Cell* **2009**, *21*, 3226–3244. [CrossRef] [PubMed]
97. Kasahara, M.; Swartz, T.E.; Olney, M.A.; Onodera, A.; Mochizuki, N.; Fukuzawa, H.; Asamizu, E.; Tabata, S.; Kanegae, H.; Takano, M.; et al. Photochemical properties of the flavin mononucleotide-binding domains of the phototropins from Arabidopsis, rice, and Chlamydomonas reinhardtii. *Plant. Physiol.* **2002**, *129*, 762–773. [CrossRef]
98. Vanhaelewyn, L.; Schumacher, P.; Poelman, D.; Fankhauser, C.; Van Der Straeten, D.; Vandenbussche, F. REPRESSOR OF ULTRAVIOLET-B PHOTOMORPHOGENESIS function allows efficient phototropin mediated ultraviolet-B phototropism in etiolated seedlings. *Plant. Sci.* **2016**, *252*, 215–221. [CrossRef] [PubMed]

99. Chapman, H.N.; Fromme, P.; Barty, A.; White, T.A.; Kirian, R.A.; Aquila, A.; Hunter, M.S.; Schulz, J.; DePonte, D.P.; Weierstall, U.; et al. Femtosecond X-ray protein nanocrystallography. *Nature* **2011**, *470*, 73–77. [CrossRef]
100. Grünbein, M.L.; Kovacs, G.N. Sample delivery for serial crystallography at free-electron lasers and synchrotrons. *Acta Crystallogr. Sect. D Struct. Biol.* **2019**, *75*, 178–191. [CrossRef] [PubMed]
101. Hart, P.; Boutet, S.; Carini, G.; Dubrovin, M.; Duda, B.; Fritz, D.; Haller, G.; Herbst, R.; Herrmann, S.; Kenney, C.; et al. The CSPAD megapixel x-ray camera at LCLS. In *SPIE Optical Engineering + Applications*; Moeller, S.P., Yabashi, M., Hau-Riege, S.P., Eds.; International Society for Optics and Photonics: Bellingham, WA, USA, 2012; p. 85040C.
102. Denes, P.; Schmitt, B. Pixel detectors for diffraction-limited storage rings. *J. Synchrotron. Radiat.* **2014**, *21*, 1006–1010. [CrossRef] [PubMed]
103. Hülsen, G.; Broennimann, C.; Eikenberry, E.F.; Wagner, A. Protein crystallography with a novel large-area pixel detector. *J. Appl. Crystallogr.* **2006**, *39*, 550–557. [CrossRef]
104. Allahgholi, A.; Becker, J.; Bianco, L.; Delfs, A.; Dinapoli, R.; Goettlicher, P.; Graafsma, H.; Greiffenberg, D.; Hirsemann, H.; Jack, S.; et al. AGIPD, a high dynamic range fast detector for the European XFEL. *J. Instrum.* **2015**, *10*, C01023. [CrossRef]
105. Casanas, A.; Warshamanage, R.; Finke, A.D.; Panepucci, E.; Olieric, V.; Nöll, A.; Tampé, R.; Brandstetter, S.; Förster, A.; Mueller, M.; et al. EIGER detector: Application in macromolecular crystallography: *Acta Crystallogr. Sect. D Struct. Biol.* **2016**, *72*, 1036–1048.